Scientific Research Publishing

Graphene, 2020, 9, 1-12
https://www.scirp.org/journal/graphene
ISSN Online: 2169-3471
ISSN Print: 2169-3439

Hydrogen Adsorption Mechanism of SiC Nanocones

M. A. Al-Khateeb[1*], A. A. El-Barbary[2,3]

[1]Physics Department, Faculty of Education and Science, Taiz University, Taiz, Yemen
[2]Physics Department, Ain-Shams University, Cairo, Egypt
[3]Physics Department, Jazan University, Jazan, Kingdom of Saudi Arabia
Email: *m_alkhateeb77@yahoo.com

How to cite this paper: Al-Khateeb, M.A. and El-Barbary, A.A. (2020) Hydrogen Adsorption Mechanism of SiC Nanocones. *Graphene*, **9**, 1-12.
https://doi.org/10.4236/graphene.2020.91001

Received: January 20, 2020
Accepted: January 28, 2020
Published: January 31, 2020

Abstract

Due to rapid depletion of fossil energy sources and increasing the environmental pollution through high fossil energy consumption, an alternative renewable and clean energy carrier as hydrogen is requested more investigations in order to get the optimal request by DOE. In this study, a deepest study on SiC nanocones is done including both of the geometrical and electronic properties of all possible five different disclination angles as a function of size using density functional (DFT) calculations at the B3LYP/6-31g level of theory. Then the hydrogen adsorption mechanism is investigated on three different sites: H^{S1} (above the first neighbor atom of the apex atoms), H^{S2} (above one atom of the apex atoms) and H^{S3} (above one atom far from the apex atoms). Our calculations show that the most candidate SiC nanocone structure for hydrogen storage is $Si_{41}N_{49}H_{10}$-HS^2-M1-Type 2 with disclination angle 300˚. In addition, our results indicate that the hydrogen adsorption induced the energy gap to decrease. Hence, these results indicate that the SiCNCs can be considered as a good candidate for hydrogen storage.

Keywords

SiCNCs, Density Functional Theory, Hydrogen Storage, Surface Reactivity

1. Introduction

Nanomaterials can find a great number of applications in modern-day technology, ranging from household to on-board satellite electronics. Because of the increasing need for speed and miniaturization of electronic devices, nanotechnology has become a very active field of study [1]-[6]. Since the discovery of carbon nanotubes (CNTs) [7], owing to their extraordinary properties, researchers have

taken much interest in exploring the immature feature and the potential applications of CNTs and also those of the related carbon nanomaterials [8] [9] [10]. Carbon nanocones (CNCs) are one of these nanomaterials. Because CNCs have structures similar to those of the CNTs and have properties much like CNTs, they have attracted much attention in recent years [11] [12]. At the same time, due to the rapid development silicon carbide SiC technology, the crystalline structure of SiC can be considered to consist of the close-packed stacking of double layers of Si and C atoms. Each C or Si atom is surrounded by four Si or C atoms in strong tetrahedral sp3 bonds. The distance between neighboring Si and C atoms is approximately 3.08 Å for all polytypes [13] [14]. The existence of SiC nanostructures that can exploit the superior physical-chemical properties of SiC [15] has been investigated and, in the last few years, many studies on SiC nanotubes have been reported in the literature [16] [17] [18]. On the contrary, little information on SiC nanocones SiCNCs is available [19]. This is unfortunate because it was proven that nanocones arrays for solar panels applications can be beneficial in terms of increased optical absorption coefficient [20]. Since space probes rely on photovoltaic power generation, solar panels based on SiCNCs arrays can be a valid alternative in terms of high-temperature, high-light intensity and high radiation conditions.

Hydrogen storage in carbon materials such as carbon nanotubes, graphite nanofibers, activated carbon and nanostructured graphite has been paid considerable attention [21]-[33]. The adsorption in carbon nanostructures seems to be the most promising method for storing hydrogen, especially on board vehicles. In particular, carbon nanotubes have been suggested as the most promising nanostructure due to its light mass density, cylindrical structure, high surface to volume ratio, as well as high degree of reactivity between the carbon and hydrogen [34] [35] [36]. Furthermore, it is well known that the adsorption of hydrogen by carbon nanotubes is temperature dependent, which can be effectively used for hydrogen uptake and release. Many experimental and theoretical efforts have been focused on hydrogen storage in carbon nanotubes [37] [38]. Recently, it has been suggested that hydrogen storage on carbon nanomaterial involves dissociation of molecular hydrogen followed by atomic hydrogen spillover. The dissociation of hydrogen takes place at transition metal sites, which are present due to residues of transition metals in the nanomaterial samples [39] [40] [41]. In this work we investigate SiCNCs with five disclination angles 60˚, 120˚, 180˚, 240˚ and 300˚. For 60˚, 180˚ and 300˚ disclination angles, there are four structures for each disclination angle of SiCNCs. However, for 120˚ and 240˚ disclination angles, there are only two structures for each disclination angle. Furthermore, the hydrogenation is done on three different sites, H^{S1} (above the first neighbor atom of the apex atoms), H^{S2} (above one atom of the apex atoms) and H^{S3} (above one atom far from the apex atoms), in addition to the study of the effect of different sizes. The adsorption energy of hydrogen as a function of cone angle, cone size and hydrogenation site are investigated. Finally, the energy gaps

(E_g), highest occupied molecular orbitals (HOMO) and lowest unoccupied molecular orbitals (LUMO), density of states (DOS), and the surface reactivity of the hydrogenations SiCNCs are investigated.

2. Methods

Density functional theory (DFT) calculations have been performed using Becke's three parameters hybrid exchange functional B3 [42] in combination with the correlation functional of Lee, Yang, and Parr (B3LYP) [43], and the 6 - 31 g standard basis set as implemented in the Gaussian 03W program [44]. All the calculations were performed by using Gauss View 4 molecular visualization program Package [45]. The samples of study are pure and mono-hydrogenated SiCNCs with five disclination angles, 60˚, 120˚, 180˚, 240˚ and 300˚. For every disclination angle, there are two structures with different sizes. For disclination angles 60˚, 180˚, and 300˚, there are two models M1 and M2 according the connected atoms edges. It can be either silicon atoms (named M1) or can be carbon atoms (named M2). For disclination angles 120˚ and 240˚, there is only one model, see **Figure 1**. The hydrogen atom can be adsorbed on silicon atom (named Type 1) or can be adsorbed on carbon atom (named Type 2). The hydrogenation is applied on three different sizes as shown in **Figure 2**. To avoid the dangling effects, the hydrogen atoms have been used to saturate the ending atoms for SiCNCs. All the atomic geometries of pure and mono-hydrogenated SiCNCs have been allowed to fully relaxation during the optimization processes. The adsorption energy of hydrogen are obtained as a function of cone angle, cone size and hydrogenation site.

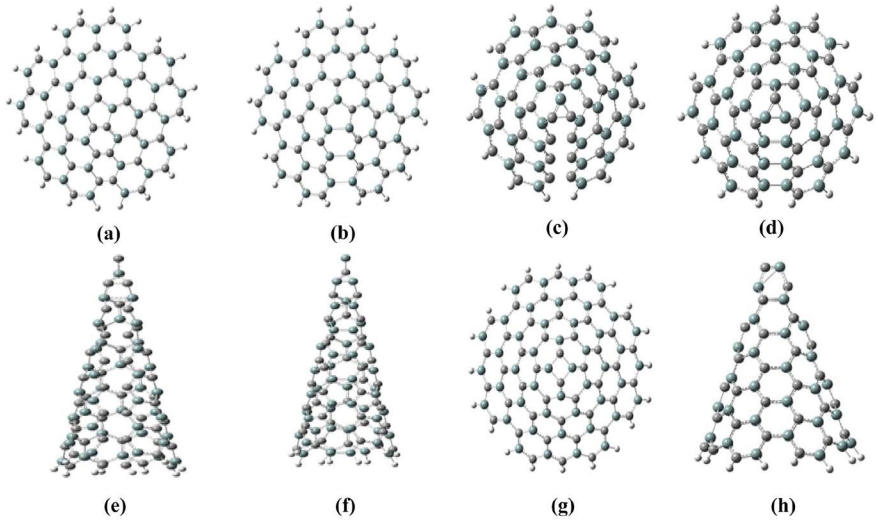

Figure 1. Optimized structures of SiCNCs: (a) $Si_{34}C_{36}$_M1 and (b) $Si_{36}C_{34}$_M2 with disclination angle 60˚; (c) $Si_{33}C_{36}$_M1 and (d) $Si_{36}C_{33}$_M2 with disclination angle 180˚; (e) $Si_{41}C_{49}$_M1 and (f) $Si_{49}C_{41}$_M2 with disclination angle 300˚; (g) $Si_{46}C_{46}$ with disclination angle 120˚; (h) $Si_{47}C_{47}$ with disclination angle 240˚ (dark cyan atoms are represented silicon atoms, grey atoms are represented carbon atoms and white atoms are represented hydrogen atoms).

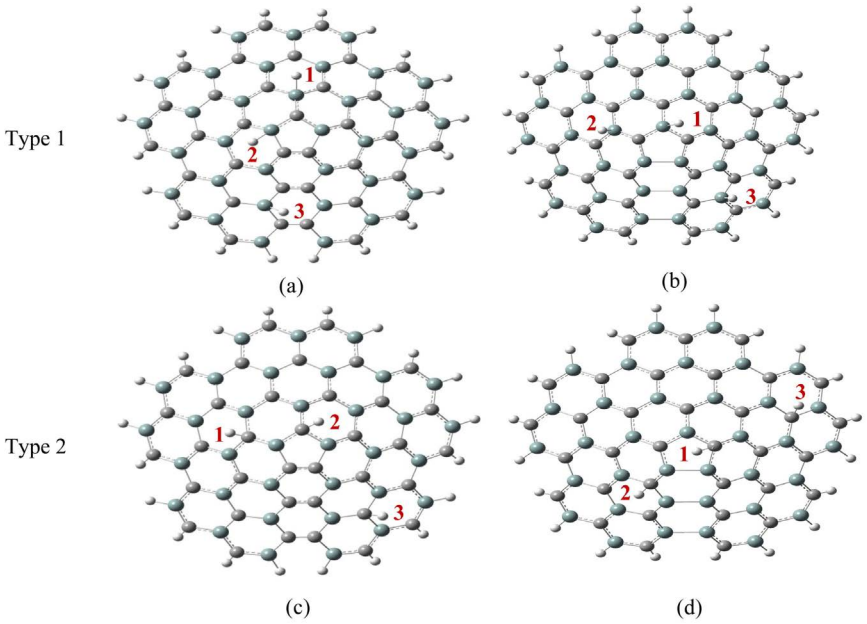

Figure 2. Schematic representation for hydrogenation sites 1-H^{S1}, 2-H^{S2}, 3-$H^{S3}$of SiCNCs with disclination angle 60˚ for structures (a) $Si_{34}C_{36}H_{20}$-M1; (b) $Si_{36}C_{34}H_{20}$-M2; (c) $Si_{56}C_{59}H_{25}$-M1 and (d) $Si_{59}C_{56}H_{25}$-M2.

3. Results and Discussion

3.1. Surface Reactivity

The surface reactivity of pure and hydrogenated SiCNCs at different disclination angels n × 60 (n = 1 to 5) and different sizes are studied. The dipole moments of pure SiCNCs are calculated and are used as indicator for the surface reactivity [46] [47], see **Table 1**. It is known that the high values of the dipole moments indicate the high surface reactivity and vice versa. From **Table 1**, the surface reactivity of SiCNCs is increased by increasing the cone size. When we increase the cone size, the rate of a chemical reaction can be raised due to the increasing surface area of nanocone. Hence, when the surface area of nanocone is increased more hydrogen atoms are expected to be adsorbed on the surface indicating the high surface reactivity. Also, it is found that the $Si_{49}C_{41}H_{10}$ (M2) with cone angle 300˚ possesses the highest surface reactivity (34.98 Debye) and the smallest surface reactivity is for $Si_{34}C_{36}H_{20}$(M1) with cone angle 60˚ (2.93 Debye). In other words, by increasing the number of silicon atoms and by decreasing the number of carbon atoms, the surface reactivity of SiCNCs is increased.

The surface reactivity of mono-hydrogenated SiCNCs at three different hydrogenation sites H^{S1} (above the first neighbor atom of the apex atoms), H^{S2} (above one atom of the apex atoms) and H^{S3} (above one atom far from the apex atoms) for both types (Type 1 and Type 2) are studied and are listed in **Table 2** and **Table 3**. One can notice that the surface reactivity of mono-hydrogenated SiCNCs are increased by increasing the cone size and by increasing the disclination angle. Also, the $Si_{49}C_{41}H_{10}$-H^{S2} (M2-Type 1) with cone angle 300˚ is found to be possess the highest surface reactivity of 36.86 Debye, and the smallest surface

Table 1. The configuration structures and the dipole moments of the SiCNCs. The dipole moment is given by Debye.

60˚		120˚		180˚		240˚		300˚	
Structures	dipole moment	Structures	dipole moment	Structures	dipole moment	Structures	dipole moment	Structures	dipole moment
$Si_{34}C_{36}H_{20}$-M1	2.93	$Si_{28}C_{28}H_{10}$	4.32	$Si_{33}C_{36}H_{15}$-M1	9.63	$Si_{23}C_{23}H_{10}$	7.22	$Si_{19}C_{24}H_{7}$-M1	12.89
$Si_{56}C_{59}H_{25}$-M1	5.03			$Si_{49}C_{53}H_{18}$-M1	14.21			$Si_{41}N_{49}H_{10}$-M1	33.24
$Si_{36}C_{34}H_{2}$-M2	3.47	$Si_{46}C_{46}H_{20}$	5.54	$Si_{36}C_{33}H_{15}$-M2	11.05	$Si_{47}C_{47}H_{14}$	17.88	$Si_{24}C_{19}H_{7}$-M2	13.41
$Si_{59}C_{56}H_{25}$-M2	5.49			$Si_{53}C_{49}H_{18}$-M2	22.28			$Si_{49}C_{41}H_{10}$-M2	34.98

Table 2. The configuration structures and the dipole moments of mono-hydrogenated SiCNCs (Type 1, Type 2), for disclination angles 120˚ and 240˚. The dipole moment is given by Debye.

120˚			240˚		
Structures	dipole moment		Structures	dipole moment	
	Type 1	Type 2		Type 1	Type 2
$Si_{28}C_{28}H_{10}$-H^{S1}	5.04	7.32	$Si_{23}C_{23}H_{10}$-H^{S1}	7.26	9.59
$Si_{28}C_{28}H_{10}$-H^{S2}	7.81	4.00	$Si_{23}C_{23}H_{10}$-H^{S2}	6.43	3.85
$Si_{28}C_{28}H_{10}$-H^{S3}	5.42	7.49	$Si_{23}C_{23}H_{10}$-H^{S3}	6.55	11.20
$Si_{46}C_{46}H_{20}$-H^{S1}	6.19	8.66	$Si_{47}C_{47}H_{14}$-H^{S1}	20.60	18.97
$Si_{46}C_{46}H_{20}$-H^{S2}	8.30	9.57	$Si_{47}C_{47}H_{14}$-H^{S2}	18.73	17.12
$Si_{46}C_{46}H_{20}$-H^{S3}	6.30	3.94	$Si_{47}C_{47}H_{14}$-H^{S3}	19.94	17.91

Table 3. The configuration structures and the dipole moments of mono-hydrogenated SiCNCs (M1-M2) and (Type 1, Type 2), for disclination angles 60˚, 180˚ and 300˚. The dipole moment is given by Debye.

Structures		dipole moment		Structures		dipole moment	
		Type 1	Type 2			Type 1	Type 2
60˚ M1	$Si_{34}C_{36}H_{20}$-H^{S1}	4.63	7.44	60˚ M2	$Si_{36}C_{34}H_{20}$-H^{S1}	7.86	9.41
	$Si_{34}C_{36}H_{20}$-H^{S2}	6.02	7.85		$Si_{36}C_{34}H_{20}$-H^{S2}	9.07	4.88
	$Si_{34}C_{36}H_{20}$-H^{S3}	3.04	7.98		$Si_{36}C_{34}H_{20}$-H^{S3}	5.15	4.03
	$Si_{56}C_{59}H_{25}$-H^{S1}	7.72	13.13		$Si_{59}C_{56}H_{25}$-H^{S1}	14.50	11.39
	$Si_{56}C_{59}H_{25}$-H^{S2}	6.81	13.64		$Si_{59}C_{56}H_{25}$-H^{S2}	13.24	10.92
	$Si_{56}C_{59}H_{25}$-H^{S3}	12.13	17.78		$Si_{59}C_{56}H_{25}$-H^{S3}	22.00	9.64
180˚ M1	$Si_{33}C_{36}H_{15}$-H^{S1}	10.46	13.48	180˚ M2	$Si_{36}C_{33}H_{15}$-H^{S1}	13.01	13.02
	$Si_{33}C_{36}H_{15}$-H^{S2}	9.39	9.15		$Si_{36}C_{33}H_{15}$-H^{S2}	10.71	7.80
	$Si_{33}C_{36}H_{15}$-H^{S3}	6.81	21.10		$Si_{36}C_{33}H_{15}$-H^{S3}	13.20	11.61
	$Si_{49}C_{53}H_{18}$-H^{S1}	17.62	14.61		$Si_{53}C_{49}H_{18}$-H^{S1}	14.03	14.80
	$Si_{49}C_{53}H_{18}$-H^{S2}	11.47	11.98		$Si_{53}C_{49}H_{18}$-H^{S2}	18.51	10.74
	$Si_{49}C_{53}H_{18}$-H^{S3}	14.91	20.90		$Si_{53}C_{49}H_{18}$-H^{S3}	14.61	10.76
300˚ M1	$Si_{19}C_{24}H_{7}$-H^{S1}	14.00	13.17	300˚ M2	$Si_{24}C_{19}H_{7}$-H^{S1}	3.49	3.45
	$Si_{19}C_{24}H_{7}$-H^{S2}	12.22	9.24		$Si_{24}C_{19}H_{7}$-H^{S2}	6.21	5.02
	$Si_{19}C_{24}H_{7}$-H^{S3}	8.67	13.91		$Si_{24}C_{19}H_{7}$-H^{S3}	4.53	4.06
	$Si_{41}C_{49}H_{10}$-H^{S1}	9.73	4.20		$Si_{49}C_{41}H_{10}$-H^{S1}	16.57	16.32
	$Si_{41}C_{49}H_{10}$-H^{S2}	4.26	9.20		$Si_{49}C_{41}H_{10}$-H^{S2}	36.86	17.65
	$Si_{41}C_{49}H_{10}$-H^{S3}	13.09	13.48		$Si_{49}C_{41}H_{10}$-H^{S3}	11.14	13.14

reactivity is found for $Si_{34}C_{36}H_{20}$-H^{S3} (M1-Type 1) with cone angle 60˚ of 3.04 Debye. Finally, it can be reported that the surface reactivity for pure and mono-hydrogenated SiCNCs is increased by increasing the cone angle and the cone size. Also, it is found that the surface reactivity is increased by hydrogenation and the highest surface reactivity is found to be 36.86 Debye for $Si_{49}N_{41}H_{10}$-H^{S2} (M2) when the hydrogenation is applied on the silicon atom (Type 1), agreed with the previous experimental finding for the effect of curvature of nanotubes in increasing the hydrogen storage capacity of more than 7 wt %, with respect to normal sheet through the formation of reversible hydrogen bonds [48].

3.2. Adsorption Energy

The adsorption energy of one hydrogen atom on the surface of SiCNCs is applied at three different hydrogenation sites H^{S1}, H^{S2} and H^{S3}. The hydrogen atom can be adsorbed on silicon atom (named Type 1) or can be adsorbed on carbon atom (named Type 2), as shown in **Figure 2**. From **Table 4** and **Table 5**, it is clear that the best hydrogenation site is H^{S2} and the adsorption energy for mono-hydrogenated SiCNCs for Type 2 is always more lower than the adsorption energy for Type 1. For disclination angle 120˚, 240˚, the best adsorption energies are found to be −2.74 eV and −4.64 eV, respectively.

However for disclination angles 60˚, 180˚ and 300˚, the best adsorption energies are found to be −1.89 eV, −4.12 eV and −4.69 eV, respectively. Finally, it is found that the adsorption energy is getting more lower by increasing the size and disclination angle of mono-hydrogenated SiCNCs, agrees with previous calculations [1] [22].

Therefore, the lowest adsorption energy is obtained for $Si_{41}N_{49}H_{10}$-H^{S2}-M1-Type 2 with disclination angle 300˚.

Table 4. The configuration structures, adsorption energy and the energy gap of mono-hydrogenated SiCNCs-Type 1 and Type 2 for disclination angles 120˚ and 240˚. All energies are given by eV.

120˚					240˚				
structure	E_{ads}^{H} (eV)		Eg (eV)		Structure	E_{ads}^{H} (eV)		Eg (eV)	
	Type 1	Type 2	Type 1	Type 2		Type 1	Type 2	Type 1	Type 2
$Si_{28}C_{28}H_{10}$-H^{S1}	−1.44	−1.48	0.09	0.04	$Si_{23}C_{23}H_{10}$-H^{S1}	−1.93	−3.53	0.04	0.04
$Si_{28}C_{28}H_{10}$-H^{S2}	−1.67	−2.74	0.10	0.04	$Si_{23}C_{23}H_{10}$-H^{S2}	−2.73	−4.58	0.06	0.06
$Si_{28}C_{28}H_{10}$-H^{S3}	−0.63	−0.46	0.10	0.03	$Si_{23}C_{23}H_{10}$-H^{S3}	−0.73	−1.54	0.05	0.02
$Si_{46}C_{46}H_{20}$-H^{S1}	−0.09	−0.42	0.08	0.03	$Si_{47}C_{47}H_{14}$-H^{S1}	−0.59	−4.12	0.02	0.01
$Si_{46}C_{46}H_{20}$-H^{S2}	−0.54	−1.56	0.08	0.04	$Si_{47}C_{47}H_{14}$-H^{S2}	−3.29	−4.64	0.03	0.02
$Si_{46}C_{46}H_{20}$-H^{S3}	0.78	0.76	0.08	0.02	$Si_{47}C_{47}H_{14}$-H^{S3}	−1.28	−1.55	0.02	0.01

Table 5. The configuration structures, adsorption energy and the energy gap of mono-hydrogenated SiCNCs (M1, M2), (Type 1, Type 2), for disclination angles 60˚, 180˚ and 300˚, All energies are given by eV.

Structures		E_{ads}^{H} (eV)		Eg (eV)		Structure		E_{ads}^{H} (eV)		Eg (eV)	
		Type 1	Type 2	Type 1	Type 2			Type 1	Type 2	Type 1	Type 2
60˚ M1	$Si_{34}C_{36}H_{20}$-H^{S1}	−1.51	−0.88	0.11	0.04	60˚ M2	$Si_{36}C_{34}H_{20}$-H^{S1}	−0.83	−0.61	0.10	0.02
	$Si_{34}C_{36}H_{20}$-H^{S2}	−1.29	−1.77	0.12	0.06		$Si_{36}C_{34}H_{20}$-H^{S2}	−1.35	−1.47	0.11	0.03
	$Si_{34}C_{36}H_{20}$-H^{S3}	−0.52	−0.28	0.06	0.06		$Si_{36}C_{34}H_{20}$-H^{S3}	−0.50	−0.41	0.11	0.05
	$Si_{56}C_{59}H_{25}$-H^{S1}	−0.55	−2.14	0.04	0.03		$Si_{59}C_{56}H_{25}$-H^{S1}	−0.81	−1.03	0.03	0.02
	$Si_{56}C_{59}H_{25}$-H^{S2}	−1.41	−1.89	0.04	0.03		$Si_{59}C_{56}H_{25}$-H^{S2}	−1.50	−1.66	0.03	0.05
	$Si_{56}C_{59}H_{25}$-H^{S3}	−0.19	−0.22	0.05	0.02		$Si_{59}C_{56}H_{25}$-H^{S3}	−0.86	−0.17	0.04	0.03
180˚ M1	$Si_{33}C_{36}H_{15}$-H^{S1}	−1.49	−1.68	0.02	0.02	180˚ M2	$Si_{36}C_{33}H_{15}$-H^{S1}	−1.98	−1.98	0.04	0.04
	$Si_{33}C_{36}H_{15}$-H^{S2}	−3.23	−4.12	0.03	0.04		$Si_{36}C_{33}H_{15}$-H^{S2}	−3.05	−3.26	0.05	0.05
	$Si_{33}C_{36}H_{15}$-H^{S3}	−0.21	−0.43	0.06	0.02		$Si_{36}C_{33}H_{15}$-H^{S3}	−0.28	−0.80	0.01	0.03
	$Si_{49}C_{53}H_{18}$-H^{S1}	−2.62	−2.07	0.03	0.04		$Si_{53}C_{49}H_{18}$-H^{S1}	−1.83	−2.46	0.04	0.04
	$Si_{49}C_{53}H_{18}$-H^{S2}	−2.12	−3.20	0.04	0.04		$Si_{53}C_{49}H_{18}$-H^{S2}	−3.35	−3.85	0.04	0.04
	$Si_{49}C_{53}H_{18}$-H^{S3}	−0.63	−1.01	0.04	0.04		$Si_{53}C_{49}H_{18}$-H^{S3}	−0.49	−0.39	0.04	0.02
300˚ M1	$Si_{19}C_{24}H_{7}$-H^{S1}	−3.09	−2.71	0.02	0.03	300˚ M2	$Si_{24}C_{19}H_{7}$-H^{S1}	−3.02	−4.10	0.02	0.02
	$Si_{19}C_{24}H_{7}$-H^{S2}	−2.05	−3.91	0.03	0.03		$Si_{24}C_{19}H_{7}$-H^{S2}	−1.76	−2.82	0.03	0.02
	$Si_{19}C_{24}H_{7}$-H^{S3}	−1.02	−1.67	0.08	0.02		$Si_{24}C_{19}H_{7}$-H^{S3}	−1.80	−1.95	0.02	0.02
	$Si_{41}C_{49}H_{10}$-H^{S1}	−3.65	−3.59	0.02	0.02		$Si_{49}C_{41}H_{10}$-H^{S1}	−3.46	−4.32	0.02	0.02
	$Si_{41}C_{49}H_{10}$-H^{S2}	−2.96	−4.69	0.03	0.01		$Si_{49}C_{41}H_{10}$-H^{S2}	−2.19	−3.57	0.03	0.02
	$Si_{41}C_{49}H_{10}$-H^{S3}	−1.02	−1.43	0.07	0.03		$Si_{49}C_{41}H_{10}$-H^{S3}	−1.79	−1.57	0.03	0.03

3.3. Valence Orbitals

The energy gaps of mono-hydrogenated SiNCs at three different hydrogenation sites H^{S1}, H^{S2} and H^{S3} for each disclination angel are studied, see **Table 4** and **Table 5**. From **Table 4**, it is found that the energy gaps for mono-hydrogenated SiCNCs-Type 2 are always smaller than the energy gaps for mono-hydrogenated SiCNCs-Type 1. The smallest and the largest energy gaps are found to be 0.01 eV for $Si_{47}C_{47}H_{14}$-H^{S3}-Type 2 with disclination angle 240˚, and 0.10 eV for $Si_{28}C_{28}H_{10}$-H^{S3}-Type 1 with disclination angle 120˚, respectively.

From **Table 5**, the energy gaps for mono-hydrogenated SiCNCs-Type 2 are always smaller than SiCNCs-Type 1. The smallest and the largest energy gaps are found to be 0.01eV and 0.12 eV for $Si_{41}C_{49}H_{10}$-H^{S2}-M1-Type 2 with disclination angle 300˚ and $Si_{34}C_{36}H_{20}$-H^{S2}-M1-Type 1 with disclination angle 60˚, respectively. In addition, it can be reported that the energy gaps for mono-hydrogenated SiCNCs when the hydrogen atom is adsorbed on carbon atom are always smaller than the energy gaps for mono-hydrogenated SiNCs when the hydrogen atom is adsorbed on silicon atom and the energy gaps before adsorption hydrogen are larger than the energy gaps after adsorption hydrogen, in a good agreement with previous observations [27] [28] [29]. From **Figure 3**, the electron density is found

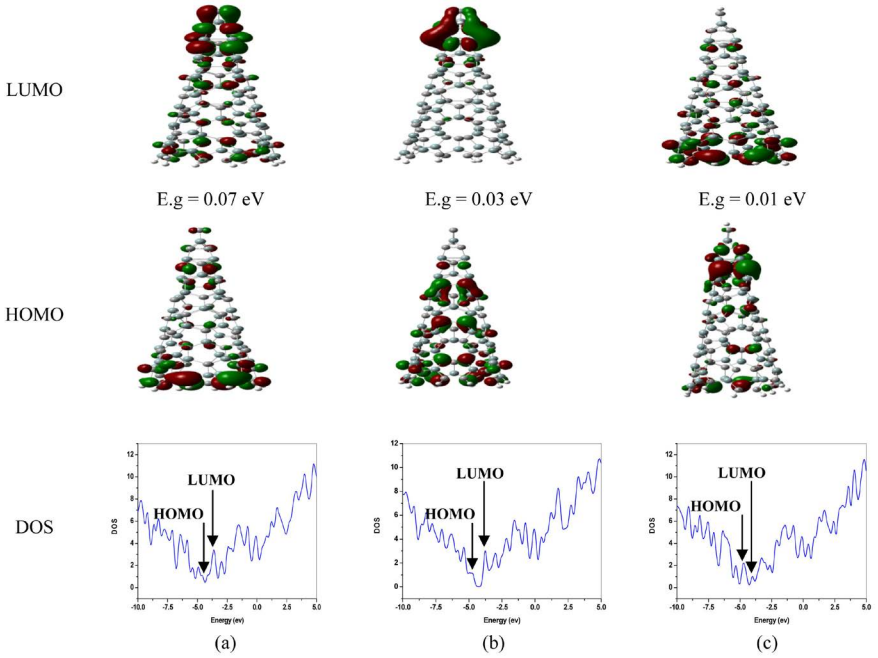

Figure 3. HOMOs, LUMOs and density of states for pure and mono-hydrogenation $Si_{41}C_{49}H_{10}$-M1-300˚, (a) $Si_{41}C_{49}$_M1; (b) $Si_{41}C_{49}H_{10}$-H^{S2}-M1-Type 1; and (c) $Si_{41}C_{49}H_{10}$-H^{S2}-M1-Type 2.

to be located at the tip of the cone for LUMO before adsorption hydrogen and after adsorption hydrogen on Type 1. However it is found to be located at the tip of the cone for HOMO after adsorption hydrogen on Type 2. Also, it is noticed that the electron density is located at terminal of the cone for the HOMO before adsorption hydrogen and after adsorption hydrogen on LUMO Type 2. The electron density is found to be distributed over most of cone for HOMO after adsorption hydrogen on Type 1. Furthermore, the intensities of the LUMOs are found to be larger than the intensities of HOMOs before and after the adsorption hydrogen on Type 1. The intensity of the LUMO is smaller than the intensity of HOMO after adsorption hydrogen on Type 2.

4. Conclusion

We have performed the adsorption energy and electronic properties of SiCNCs using the DFT calculations. It is found that the adsorption energy is getting lower by increasing the size and disclination angle of mono-hydrogenated SiCNCs. The more lower adsorption energy is found to be −4.69 eV for $Si_{41}N_{49}H_{10}$-H^{S2}-M1-Type 2 with disclination angle 300˚. Also, the energy gaps for mono-hydrogenated SiCNCs when the hydrogen atom is adsorbed on carbon atom are always smaller than the energy gaps for mono-hydrogenated SiNCs when the hydrogen atom is adsorbed on silicon atom where the smallest energy gap is 0.01 eV for $Si_{41}C_{49}H_{10}$-H^{S2}-M1-Type 2 with disclination angle 300˚. Finally, the surface reactivity is found to be increased by hydrogenation where the highest surface reactivity is found to be (36.86 Debye) for $Si_{49}N_{41}H_{10}$-H^{S2} (M2) when the hydro-

genation is applied on the silicon atom (Type 1). Both the high surface area and the opportunity for SiCNCs consolidation are key attributes for hydrogen storage devices and lead to the design of light weight hydrogen storage systems with better hydrogen storage characteristics. Hence, more investigations of the capabilities of SiCNCs for the physicochemical reactions, such as surface interactions and hydrogen atom dissociation are needed.

Conflicts of Interest

The authors declare no conflicts of interest regarding the publication of this paper.

References

[1] El-Barbary, A.A., Kamel, M.A., Eid, K.M., Taha, H.O., Mohamed, R.A. and Al-Khateeb, M.A. (2015) The Surface Reactivity of Pure and Monohydrogenated Nanocones Formed from Graphene Sheets. *Graphene*, **45**, 75-83. https://doi.org/10.4236/graphene.2015.44008

[2] El-Barbary, A.A., Kamel, M.A., Eid, K.M., Taha, H.O. and Hassan, M.M. (2015) Mono-Vacancy and B-Doped Defects in Carbon Heterojunction Nanodevices. *Graphene*, **4**, 84-90. https://doi.org/10.4236/graphene.2015.44009

[3] El-Barbary, A.A., Eid, K.M., Kamel, M.A., Taha, H.O. and Ismail, G.H. (2015) Adsorption of CO, CO_2, NO and NO_2 on Boron Nitride Nanotubes: DFT Study. *Journal of Surface Engineered Materials and Advanced Technology*, **5**, 154-161. https://doi.org/10.4236/jsemat.2015.53017

[4] El-Barbary, A.A., Eid, K.M., Kamel, M.A., Taha, H.O. and Ismail, G.H. (2015) Adsorption of CO, CO_2, NO and NO_2 on Carbon Boron Nitride Hetero Junction: DFT Study. *Journal of Surface Engineered Materials and Advanced Technology*, **5**, 169-176. https://doi.org/10.4236/jsemat.2015.54019

[5] El-Barbary, A.A., Eid, K.M., Kamel, M.A., Taha, H.O. and Ismail, G.H. (2014) Effect of Tubular Chiralities and Diameters of Single Carbon Nanotubes on Gas Sensing Behavior: A DFT Analysis. *Journal of Surface Engineered Materials and Advanced Technology*, **4**, 66-74. https://doi.org/10.4236/jsemat.2014.42010

[6] El-Barbary, A.A., Ismail, G.H. and Babaier, A. (2013) Theoretical Study of Adsorbing CO, CO_2, NO and NO_2 on Carbon Nanotubes. *Journal of Surface Engineered Materials and Advanced Technology*, **3**, 287-294. https://doi.org/10.4236/jsemat.2013.34039

[7] Iijima, S. (1991) Helical Microtubules of Graphitic Carbon. *Nature*, **354**, 56-58. https://doi.org/10.1038/354056a0

[8] El-Barbary, A.A., Telling, R.H., Ewels, C.P. and Heggie, M.I. (2003) Structural and Energetics of the Vacancy in Graphite. *Physical Review B*, **68**, Article ID: 144107. https://doi.org/10.1103/PhysRevB.68.144107

[9] Ewels, C.P., Telling, R.H., El-Barbary, A.A. and Heggie, M.I. (2003) Metastable Frenkel Pair Defect in Graphite: Source of Winger Energy. *Physical Review Letters*, **91**, Article ID: 025505. https://doi.org/10.1103/PhysRevLett.91.025505

[10] Telling, R.H., Ewels, C.P., El-Barbary, A.A. and Heggie, M.I. (2003) Wigner Defects Bridge the Graphite Gap. *Nature Materials*, **2**, 333-337. https://doi.org/10.1038/nmat876

[11] Sattler, K. (1995) Scanning Tunneling Microscopy of Carbon Nanotubes and Nanocones. *Carbon*, **33**, 915-920. https://doi.org/10.1016/0008-6223(95)00020-E

[12] Garberg, S.N., Naess, G., Helgesen, K.D., Knudsen, G., Kopstad, A. and Elgsaeter, A. (2008) Transmission Electron Microscopeand Electron Diraction Study of Carbon Nanodisks. *Carbon*, **46**, 1535-1543. https://doi.org/10.1016/j.carbon.2008.06.044

[13] Harris, G.L. (1995) Properties of Silicon Carbide. INSPEC, the Institution of Electrical Engineers, London.

[14] Zetterling, C.M. (2002) Process Technology for Silicon Carbide Devices. IET, London. https://doi.org/10.1049/PBEP002E

[15] Matsunami, H. (2004) Technological Breakthroughs in Growth Control of Silicon Carbide for High Power Electronic Devices. *Japanese Journal of Applied Physics*, **43**, 6835. https://doi.org/10.1143/JJAP.43.6835

[16] Wu, J.J. and Guo, G.Y. (2007) Optical Properties of SiC Nanotubes: An *Ab initio* Study. *Physical Review B*, **76**, Article ID: 035343. https://doi.org/10.1103/PhysRevB.76.035343

[17] Gali, A. (2006) *Ab initio* Study of Nitrogen and Boron Substitutional Impurities in Single-Wall SiC Nanotubes. *Physical Review B*, **73**, Article ID: 245415. https://doi.org/10.1103/PhysRevB.73.245415

[18] Alfieri, G. and Kimoto, T. (2009) The Structural and Electronic Properties of Chiral SiC Nanotubes: A Hybrid Density Functional Study. *Nanotechnology*, **20**, Article ID: 285703. https://doi.org/10.1088/0957-4484/20/28/285703

[19] Mavrandonakis, A., Froudakis, G.E., Andriotis, A. and Menon, M. (2006) Silicon Carbide Nanotube Tips: Promising Materials for Atomic Force Microscopy and/or Scanning Tunneling Microscopy. *Physical Review Letters*, **89**, Article ID: 123126. https://doi.org/10.1063/1.2221418

[20] Zhu, J., Yu, Z., Burkhard, G.F., Hsu, C.M., Connor, S.T., Xu, Y., Wang, Q., McGehee, M., Fan, S. and Cui, Y. (2009) Optical Absorption Enhancement in Amorphous Silicon Nanowire and Nanocone Arrays. *Nano Letters*, **9**, 279-282. https://doi.org/10.1021/nl802886y

[21] El-Barbary, A.A. (2019) Hydrogen Storage on Cross Stacking Nanocones. *International Journal of Hydrogen Energy*, **44**, Article ID: 20099. https://doi.org/10.1016/j.ijhydene.2019.05.043

[22] El-Barbary, A.A. and Al-Khateeb, M.A. (2018) A Theoretical Study of Hydrogen Adsorption on Surface Nanocone Materials. *Current Science International*, **7**, 370-375.

[23] EL-Barbary, A.A. (2018) Vacancy Cluster in Graphite: Migration Mechanism and Aggregation. *AIP Conference Proceedings*, **1976**, Article ID: 020006. https://doi.org/10.1063/1.5042373

[24] EL-Barbary, A.A. (2017) New Insights into Canted Spiro Carbon Interstitial in Graphite. *Applied Surface Science*, **426**, 238-243. https://doi.org/10.1016/j.apsusc.2017.07.196

[25] EL-Barbary, A.A. (2016) Hydrogenated Fullerenes in Space: FT-IR Spectra Analysis. *AIP Conference Proceedings*, **1742**, Article ID: 030005. https://doi.org/10.1063/1.4953126

[26] EL-Barbary, A.A. (2016) Hydrogenated Fullerenes Dimer, Peanut and Capsule: An Atomic Comparison. *Applied Surface Science*, **369**, 50-57. https://doi.org/10.1016/j.apsusc.2016.02.033

[27] EL-Barbary, A.A. (2016) Potential Energy of H_2 inside the C_{116} Fullerene Dimerization: An Atomic Analysis. *Journal of Molecular Structure*, **1112**, 9-13. https://doi.org/10.1016/j.molstruc.2016.02.007

[28] EL-Barbary, A.A. (2016) Hydrogenation Mechanism of Small Fullerene Cages. *International Journal of Hydrogen Energy*, **41**, 375-383. https://doi.org/10.1016/j.ijhydene.2015.10.102

[29] EL-Barbary, A.A. (2015) The Surface Reactivity and Electronic Properties of Small Hydrogenation Fullerene Cages. *Journal of Surface Engineered Materials and Advanced Technology*, **5**, 162-168. https://doi.org/10.4236/jsemat.2015.53018

[30] EL-Barbary, A.A. (2015) ^{1}H and ^{13}C NMR Chemical Shift Investigations of Hydrogenated Small Fullerene Cages C_n, C_nH, C_nH_n and C_nH_{n+1}: n=20, 40, 58, 60. *Journal of Molecular Structure*, **1097**, 76-86. https://doi.org/10.1016/j.molstruc.2015.05.015

[31] EL-Barbary, A.A. and Hindi, A.A. (2015) Hydrogen Storage on Halogenated C_{40} Cage: An Intermediate between Physisorption and Chemisorptions. *Journal of Molecular Structure*, **1080**, 169-175. https://doi.org/10.1016/j.molstruc.2014.09.034

[32] El-Barbary, A.A., Eid, K.M., Al-Khateeb, M.A. and Kamel, M.A. (2010) The Role of Irradiation in Graphite for Hydrogen Storage. *Arab Journal of Nuclear Sciences and Applications*. https://inis.iaea.org/collection/NCLCollectionStore/_Public/42/076/42076631.pdf?r=1 https://inis.iaea.org/search/search.aspx?search-option=everywhere&orig_q=The%20role%20of%20irradiation%20in%20graphite%20for%20hydrogen%20storage

[33] El-Barbary, A.A., Lebda, H.I. and Kamel, M.A. (2009) The High Conductivity of Defect Fullerene C_{40} Cage. *Computational Materials Science*, **46**, 128-132. https://doi.org/10.1016/j.commatsci.2009.02.034

[34] Berry, G.D. and Aceves, S.M. (1998) Onboard Storage Alternatives for Hydrogen Vehicles. *Energy Fuels*, **12**, 49-55. https://doi.org/10.1021/ef9700947

[35] Chen, P., Wu, X., Lin, J. and Tan, K.L. (1999) High H2 Uptake by Alkali-Doped Carbon Nano Tubes under Ambient Pressure and Moderate Temperatures. *Science*, **285**, 91-93.

[36] Liu, C. and Cheng, H.M. (2005) Carbon Nanotubes for Clean Energy Applications. *Journal of Physics D: Applied Physics*, **38**, 231-252. https://doi.org/10.1088/0022-3727/38/14/R01

[37] Strobel, R., Garche, J., Moseley, P.T., Jorissen, L. and Wolf, G. (2006) Hydrogen Storage by Carbon Materials. Journal of Power Sources, **159**, 781-801. https://doi.org/10.1016/j.jpowsour.2006.03.047

[38] Baughman, R.H., Zakhidov, A.A. and De Heer, W.A. (2002) Carbon Nanotubes—The Route toward Applications. *Science*, **297**, 787-792. https://doi.org/10.1126/science.1060928

[39] Yang, F.H. and Yang, R.T. (2002) Adsorption Behaviors of HiPco Single-Walled Carbon Nanotube Aggregates for Alcohol Vapors. *The Journal of Physical Chemistry*, **106**, 8994-8999.

[40] Zhao, Y., Kim, Y.H., Dillon, A.C., Heben, M.J. and Zhang, S.B. (2005) *Ab initio* Design of Ca-Decorated Organic Frameworks for High Capacity Molecular Hydrogen Storage with Enhanced Binding. *Physical Review Letters*, **95**, Article ID: 155504. https://doi.org/10.1103/PhysRevLett.94.155504

[41] Yang, F.H., Lachawiec, A.J. and Yang, R.T. (2006) Hydrogen Sorption on Palladium-Doped Sepiolite-Derived Carbon Nanofibers. *The Journal of Physical Chemistry B*, **110**, 6236-6244. https://doi.org/10.1021/jp056461u

[42] Becke, A.D. (1993) Density-Functional Thermochemistry. III. The Role of Exact Exchange. *Chemical Physics*, **98**, 5648. https://doi.org/10.1063/1.464913

[43] Vosko, S.H., Wilk, L., Nusair, M. and Can, J. (1980) Influence of an Improved Local-Spin-Density Correlation-Energy Functional on the Cohesive Energy of Alkali Metals. *Physical Review B*, **22**, 3812-3815. https://doi.org/10.1103/PhysRevB.22.3812

[44] Frisch, M.J., Trucks, G.W., Schlegel, H.B., Scuseria, G.E., Robb, M.A., Cheeseman, J.R., Zakrzewski, V.G., Montgomery, J.A., Stratmann, R.E., Burant, J.C., Dapprich, S., Millam, J.M., Daniels, A.D., Kudin, K.N., Strain, M.C., Farkas, O., Tomasi, J., Barone, V., Cossi, M., Cammi, R., Mennucci, B., Pomelli, C., Adamo, C., Clifford, S., Ochterski, J., Petersson, G.A., Ayala, P.Y., Cui, Q., Morokuma, K., Malick, D.K., Rabuck, A.D., Raghavachari, K., Foresman, J.B., Cioslowski, J., Ortiz, J.V., Stefanov, B.B., Liu, G., Liashenko, A., Piskorz, P., Komaromi, I., Gomperts, R., Martin, R.L., Fox, D.J., Keith, T., Al-Lamham, M., Peng, C.Y., Nanayakkara, A., Gonzalez, C., Challacombe, M., Gill, P.M.W., Johnson, B.G., Chen, W., Wong, M.W., Andres, J.L., Head-Gordon, M., Replogle, E.S. and Pople, J.A. (2004) Gaussian 2004. Gaussian Inc., Wallingford.

[45] Frisch, A., Dennington, R.D., Keith, T.A., Millam, J., Nielsen, A.B., Holder, A.J. and Hiscocks, J. (2003) Gauss View Manual Version 4. Gaussian Inc.

[46] El-Nahass, M.M., Kamel, M.A., El-Barbary, A.A., El-Mansy, M.A.M. and Ibrahim, M. (2013) On the Spectroscopic Analyses of Thioindigo Dye. *Spectrochimica Acta Part A*: *Molecular and Biomolecular Spectroscopy*, **113**, 332-336.

[47] Kotz, J.C., Treichel, P. and Weaver, G.C. (2006) Chemistry and Chemical Reactivity. Thomson Brooks Cole, Pacific Grove.

[48] Nikitin, A., Li, X.L., Zhang, Z.Y., Ogasawara, H., Dai, H.J. and Nilsson, A. (2008) Hydrogen Storage in Carbon Nanotubes through the Formation of Stable C-H Bonds. *Nano Letters*, **8**, 162-167. https://doi.org/10.1021/nl072325k